

Atomic-Scale Observation of the Metal-Promoter Interaction in Rh-Based Syngas Upgrading Catalysts

Xing Huang,* Detre Teschner, Maria Dimitrakopoulou, Alexey Fedorov, Benjamin Frank, Ralph Kraehnert, Frank Rosowski, Harry Kaiser, Stephan Schunk, Christiane Kuretschka, Robert Schlögl, Marc-Georg Willinger* and Annette Trunschke*

Abstract: The direct conversion of syngas to ethanol is a cornerstone reaction in evolving technologies of CO₂ utilization and hydrogen storage, which is typically performed using promoted Rh catalysts. A rational catalyst development requires a detailed structural understanding of the activated catalyst and in particular, the specific roles that promoters play in driving the chemoselectivity of this process. Herein, we report for the first time a comprehensive and comparative atomic-scale study of metal-promoter interaction in silica-supported Rh, Rh-Mn and Rh-Mn-Fe catalysts by aberration-corrected transmission electron microscopy (AC-TEM). We uncover that while the catalytic reaction leads to the formation of a Rh carbide phase in the Rh-Mn/SiO₂ catalyst, the addition of Fe results in the formation of bimetallic Rh-Fe alloys. The latter further improves the selectivity and prevents the carbide formation. In all promoted catalysts, the Mn is present as oxide decorating the metal particles. Based on the atomic insight presented in this work, structural and electronic modifications induced by promoters are revealed and a basis for refined theoretical models is provided.

The direct conversion of syngas (CO+H₂) to ethanol and higher alcohols (C₂₊) is an attractive alternative to the conventional processes of ethylene hydration or biomass fermentation.^[1] Heterogeneous Rh-based catalysts are among the best systems for this process.^[2] While Rh alone provides poor selectivity to ethanol and other C₂₊ oxygenates due to the competing methanation reaction, the addition of promoters such as Mn or Fe

improves both the specific activity and the selectivity to ethanol.^[1b, 2-3] The effect of promoters has been investigated extensively experimentally^[4] and by DFT calculations,^[5] however, our present understanding of the underlying metal-promoter interaction remains very limited. It has widely been proposed that an intimate contact between the metal and a promoter is essential for inducing the so-called strong metal-promoter interaction (SMPI) that enhances the catalytic performance;^[2, 6] that said, the atomic nature of this interaction is not clear.

Structural complexity of promoted Rh-based catalysts makes the mutual interaction between the components challenging to resolve by spectroscopic tools at the atomic scale. The difficulties are primarily related to the low catalyst loading and minute concentrations of promoters.^[4a] Studying such catalysts using electron microscopy is plagued by issues, such as with the high beam sensitivity of the system and the charging effects due to the non-conductive silica support.^[7] The current lack of atomic-scale structural and compositional information, and in particular, the mechanism by which the promoters influence the catalytic function of the active Rh, is still under debate^[1a, 2, 5b, 7] and begs for more experimental and theoretical work. In the last decade, advances in high-resolution TEM yielded an unprecedented level of insight into the local atomic arrangement of the complex catalysts.^[8] Herein, we apply AC-TEM to investigate promoted Rh catalysts and systematically study the interaction between the metal and the added promoters as well as their evolution under the reaction conditions.

- [a] Dr. X. Huang, Dr. D. Teschner, Prof. Robert Schlögl
Department Heterogeneous Reactions, Max Planck Institute for Chemical Energy Conversion, Stiftstrasse 34-36, 45470 Mülheim an der Ruhr, Germany
E-mail: xinghuang0214@mail.ipc.ac.cn
- [b] Dr. X. Huang, Dr. D. Teschner, Dimitrakopoulou, Dr. MProf. Robert Schlögl, Dr. M. G. Willinger, Dr. A. Trunschke
Department of Inorganic Chemistry, Fritz-Haber-Institut der Max-Planck-Gesellschaft, Faradayweg 4-6, 14195 Berlin, Germany
E-mail: marc.willinger@scopem.ethz.ch
E-mail: trunschke@fhi-berlin.mpg.de
- [c] Dr. B. Frank, Dr. R. Kraehnert, Dr. F. Rosowski
BasCat - UniCat BASF Joint Lab, Hardenbergstraße 36, 10623 Berlin, Germany
- [d] Dr. F. Rosowski, Dr. C. Kuretschka
BASF SE, Process Research and Chemical Engineering, Heterogeneous Catalysis, Carl-Bosch-Straße 38, 67056, Ludwigshafen, Germany
- [e] Dr. H. Kaiser, Dr. S. Schunk
hte GmbH, Kurpfalzring 104, 69123 Heidelberg, Germany
- [f] Dr. A. Fedorov
Department of Mechanical and Process Engineering, ETH Zürich, Leonhardstrasse 21, 8092 Zürich, Switzerland

Supporting information for this article is given via a link at the document. [\(\(Please delete this text if not appropriate\)\)](#)

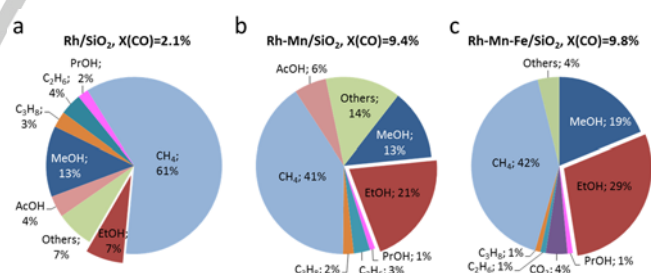


Figure 1. Selectivity and conversion in syngas upgrading over (a) Rh/SiO₂, (b) Rh-Mn/SiO₂, and (c) Rh-Mn-Fe/SiO₂ (space-time yield of 0.80 mmol ml⁻¹ min⁻¹ after 800 h TOS). Reaction conditions: 260°C, 54 bar, 60% H₂, 20% CO, 20% N₂, (a) 11667 h⁻¹, (b) 5833 h⁻¹, (c) 3889 h⁻¹. Others: C₄₊ alcohols and alkanes as well as alkenes and various oxygenates.

Three frequently studied catalysts, *i.e.* un-promoted Rh on silica, Mn promoted Rh on silica, and Mn-Fe co-promoted Rh on silica were prepared using a co-impregnation method with loadings of, respectively, 2.5 wt% Rh, 1.5 wt% Mn, and 0.5 wt% Fe. The samples were catalytically tested and investigated by TEM after calcination, reductive activation and catalytic reaction. This strategy allowed us to follow reaction induced modifications and the evolution of the metal-promoter interaction at three relevant catalyst states, as reported in details below.

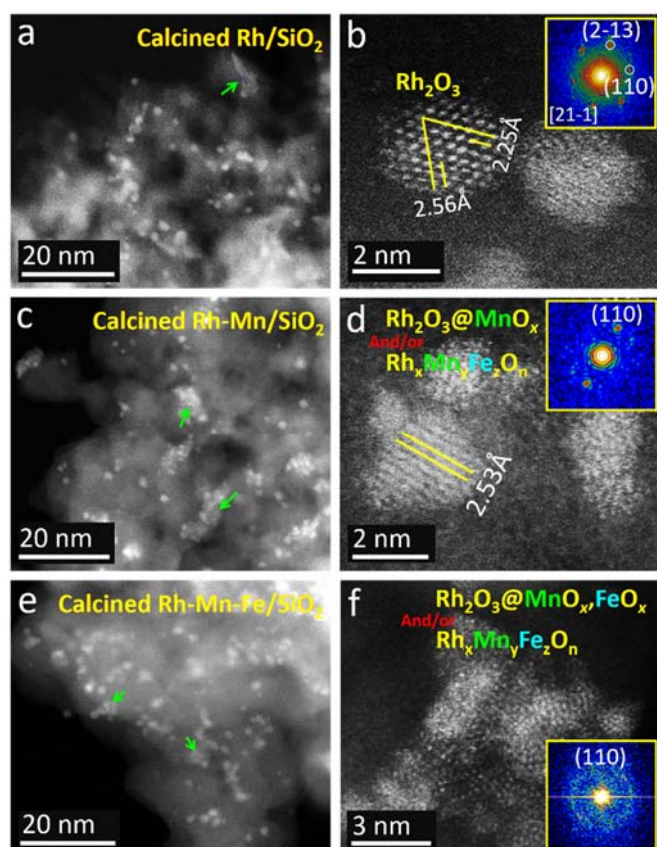


Figure 2. HAADF-STEM images of calcined (a,b) Rh/SiO₂, (c,d) Rh-Mn/SiO₂ and (e-f) Rh-Mn-Fe/SiO₂; Insets of (b,d,f) show respectively the FFTs of the corresponding nanostructures. Arrows mark the raft-like structure present in the calcined catalyst.

Catalytic testing reveals that the selectivity to ethanol increases from Rh/SiO₂ to Rh-Mn/SiO₂ and to Rh-Mn-Fe/SiO₂ (Figure 1). Mn promoter enhances both activity and selectivity, while addition of Fe as a second promoter increases the yield further due to a distinct increase in ethanol selectivity at comparable conversion. However, the Mn-Fe-promoted catalyst is less active compared to Rh-Mn/SiO₂ catalyst (Figure S1). Since our catalytic data is consistent with previous reports,^[2, 9] the synthesized catalysts can be considered as representative and suitable model catalysts for the investigation of the metal-promoter interaction and associated synergistic effects.

The morphologies and structures of the freshly calcined catalysts were first characterized by high-angle annular dark-field scanning TEM (HAADF-STEM). The HAADF-STEM image of the promoter-free Rh/SiO₂ reveals mostly crystalline Rh₂O₃ nanoparticles that are highly dispersed and homogeneously distributed over the SiO₂ surface (Figure 2a). Lattice fringes with *d*-spacings of 2.56 Å and 2.25 Å are consistent with (110) and (2-13) facets of the corundum-like Rh₂O₃ (Figure 2b).^[10] The presence of Rh₂O₃ was also confirmed by X-ray photoelectron spectroscopy (XPS, Figure S2). Besides the crystalline nanoparticles, survey of the material also reveals less abundant poorly crystalline particles of a raft-like morphology (see arrows in Figure 2a and Figure S3b for a high-resolution image of such structure). We note that these structures are very sensitive to the

electron beam and require low-dose imaging to avoid beam-induced structural modification and reduction.

The size of crystalline nanoparticles in the calcined Rh-Mn/SiO₂ (Figure 2c) and Rh-Mn-Fe/SiO₂ (Figure 2e) catalysts was comparable to that in calcined Rh/SiO₂. The observed lattice fringes are in agreement with the structure of Rh₂O₃ (Figure 2d), although local EDX analysis reveals the simultaneous presence of the promoter signal (Figure S4, Figure S5b, EDX 1). Notably, more raft-like structures were observed in the promoted catalysts (see arrows in Figures 2c,e). A representative HAADF-STEM image of such a raft-like aggregate in the calcined Rh-Mn-Fe/SiO₂ catalyst is shown in Figure 2f. The corresponding fast Fourier transformation (FFT) shows a weak and broad ring that can be indexed to the (110) reflection of Rh₂O₃ (inset in Figure 2f). EDX analysis of such structures reveals the simultaneous presence of Rh, Mn, and Fe. Although the distribution of Mn, Fe and Rh can be inhomogeneous within individual aggregates (Figure S5c-k), the close proximity of promoters and Rh indicates that the raft-like structures comprise a complex mixture of oxides. XPS analysis (Figure S2) shows that the 3d peak of Rh in both, the calcined Rh-Mn/SiO₂ and Rh-Mn-Fe/SiO₂ catalysts is slightly shifted to higher binding energies (309.2-309.3 eV) compared to the Rh peak in the calcined Rh/SiO₂ (308.9 eV). This may be due to a partial incorporation of promoters into the Rh₂O₃ matrix and formation of complex Rh_xMn_yFe_zO_n oxides. The raft-like structures are highly sensitive to the electron beam. Extended irradiation leads to the formation of metallic Rh nanoparticles that are surrounded by a layer of lower contrast which, according to EDX, consists of a binary Mn-Fe oxide (Figures S5b, EDX 2). Although in this case, the core/shell configuration was induced by electron beam reduction, this transformation may serve as a model for the chemical state that eventually evolves under reducing reaction conditions.

To conclude, we can propose a structural model for the calcined Rh-Mn-Fe/SiO₂ catalyst (Figure S5i) according to which i) the promoters are in an intimate contact with the rhodium oxide, and ii) complex mixed oxides containing Mn_xFe_yO_z doped Rh₂O₃ (Rh_xMn_yFe_zO_n) exist in the catalyst.

Next, we characterized reduced and spent catalysts. HAADF-STEM micrographs recorded after the H₂ reduction or long-term catalytic testing reveal crystalline metallic nanoparticles (Figures 3a,c and S3c,d and S6-S8). The particle size distribution is similar in all catalysts with a maximum close to 2 nm. However, some larger particles with sizes up to 20-40 nm appear in the spent catalysts (Figures S9 and S10). Since those were absent in the freshly reduced catalysts (Figures S7 and S8), we assume that they form by sintering during the catalytic reaction. A detailed analysis of the microstructures is shown in Figures 3 and Figures S3c,d and S6. The lattice fringes with a *d*-spacing of 2.23-2.25 Å correspond to the (111) planes of metallic Rh in Rh/SiO₂ (Figure S3d) and Rh-Mn/SiO₂ (Figure S6a,d). In contrast, the intensity profiles taken from the region indicated in Figures 3a,c reveal that the (111) lattice *d*-spacing of metal particles in Rh-Mn-Fe/SiO₂ is slightly decreased after both reduction and catalytic testing. This could be a result of incorporation of promoter elements into the Rh during the reduction.^[11] Indeed, the formation of Rh-Fe alloy was suggested in Fe modified Rh catalysts (Rh-Fe/TiO₂)^[12] during the syngas conversion, however, without a direct evidence for such phase.

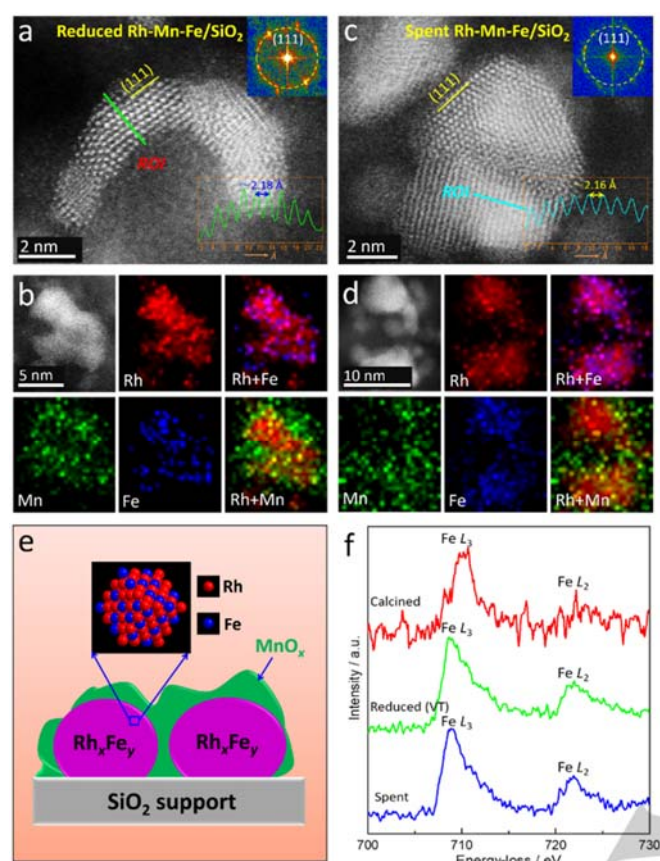


Figure 3. Structural and compositional characterization of (a,b) reduced and (c,d) spent Rh-Mn-Fe/SiO₂ catalysts. (a,c) HAADF-STEM images; insets show FFTs and intensity profiles taken from the assigned regions of interest (ROI); (b,d) HAADF-STEM images and corresponding EDX mappings; (e) Schematic model hypothesized for Rh-Mn-Fe/SiO₂ after reduction and catalytic reaction; (f) STEM-EELS spectra at the Fe *L*-edge of calcined, reduced and used Rh-Mn-Fe/SiO₂. To prevent air contact, the reduced sample was transferred from a glove box into TEM using a vacuum transfer (VT) holder.

In order to confirm the alloy formation, we analyzed the atomic composition by STEM-EDX elemental mapping. Figures 3b,d show HAADF-STEM images and corresponding EDX maps of Rh, Fe and Mn obtained from the H₂ reduced and spent catalysts. Additional EDX mapping analysis on different sized particles in the spent Rh-Mn-Fe/SiO₂ catalyst is presented in Figure S11a. Elemental mapping confirms that Rh and Fe are always distributed over the same region, thus strongly suggesting that Rh and Fe form a bimetallic alloy. In addition, EDX-line scans show that the signal intensities due to Rh and Fe are almost synchronized, which indicates a homogeneous bulk alloy structure rather than a surface alloy (Figure S11b).

In contrast, the Mn signal is distributed around the Rh-Fe particles, and thus is not involved in the alloy formation. The distribution of Mn is similar in the case of Rh-Mn/SiO₂ (Figures S6b,e) and is independent of the presence of the Fe promoter. In agreement with analyses of lattice spacing and elemental mapping, a minor binding energy shift of the Rh 3d peak to a higher energy in the XPS spectrum of the reduced and the spent Rh-Mn-Fe/SiO₂ catalyst (Figure S12b,c) suggests that the electronic structure of Rh is modified, which can be caused by the alloying with Fe. In the Rh 3d XPS spectrum of the reduced and

spent Rh-Mn/SiO₂ catalysts, the impact of Mn on the electronic structure of Rh is barely noticeable (Figure S12a). Furthermore, the amount of Fe in the Rh-Fe alloy particles was quantified by performing compositional EDX analysis on many individual particles (Figure S13). The statistical analysis indicates a Fe/Rh mass ratio of 0.1 (atomic ratio Fe/Rh=0.18) in the reduced and 0.14 (atomic ratio Fe/Rh=0.26) in the used Rh-Mn-Fe/SiO₂ catalyst, respectively. However, according to the inductively coupled plasma optical emission spectrometry (ICP-OES), the overall Fe/Rh ratio in the catalyst should be about 0.2 (atomic ratio Fe/Rh=0.36). Thus, not all of the Fe in the catalysts was forming an alloy with Rh during reduction and catalytic reaction. It is possible that some of the Fe is present as highly dispersed oxidic or sub-oxidic species after H₂ reduction and/or catalytic reaction.

We used electron energy-loss spectroscopy (EELS) to provide further evidence for the formation of the bimetallic Rh-Fe alloys. Figure 3f shows the EELS spectra of Fe *L*_{2,3} excitation edges from calcined, reduced, and spent Rh-Mn-Fe/SiO₂ catalysts, respectively. Although the Fe *L*_{2,3}-edges appear weak due to the low Fe content, the chemical position and shape of the spectra change with the pre-treatment conditions of the catalyst. Comparison of Fe *L*_{2,3} edges clearly shows that both, hydrogen treatment and catalytic reaction, lead to reduction of the iron oxide. This is manifested by the shift of the Fe *L*₃ ionization edge (defined at half maximum of the peak) from ca. 709 eV in case of the calcined sample to ca. 707.8 eV for both, the reduced and used catalyst. In fact, the preservation of the metallic state in the catalysts even after exposure to ambient conditions indicates formation of a Rh-Fe alloy, which stabilizes Fe in the metallic state.^[13] The bimetallic Rh-Fe alloy was further characterized by STEM-EELS mapping (Figure S14). Note that the temperature of H₂ reduction and catalytic reaction was much lower than typically required for the reduction of Fe oxide. Its reduction can be understood by the hydrogen spill-over: once Rh₂O₃ gets reduced by H₂ (or H₂+CO) to metallic Rh, the latter serves as a catalyst for H₂ dissociation and thus facilitates the reduction of iron oxide. In contrast, the reducibility of Mn oxide is lower, reflected by the more negative reduction potential. Hence, the Mn is likely existing as oxide in the reduced and the spent catalysts. This may explain why there is no Rh-Mn alloy formed in the Mn promoted Rh catalysts. The oxidic nature of Mn is further confirmed by XPS (Figure S15), although the oxidation state is not conclusive due to the lack of chemical shifts for the various Mn oxides.^[14]

So far, we have revealed that after the catalytic reaction sintering of nanoparticles occurs in both Mn, and Mn-Fe promoted catalysts. In the bi-promoted catalyst, the nanoparticles (including the sintered particles) have been systematically characterized and confidently demonstrated to be the Rh-Fe alloy, as discussed above. In Mn promoted catalyst, however, the morphology of sintered particles is different in comparison to that of metallic Rh, suggesting a different phase. To reveal their composition, EELS and EDX characterizations were performed. Figure 4a shows an EELS spectrum collected from the dotted line across a sintered particle in the used Rh-Mn/SiO₂ catalyst. For comparison, the EELS spectrum of a Rh-Fe alloy particle in the spent Rh-Mn-Fe/SiO₂ catalyst is also shown (Figure 4b). The O *K* edge present in both spectra is due to the silica support underneath the particles. The Mn *L* edge is recorded from the surrounding MnO_x species.

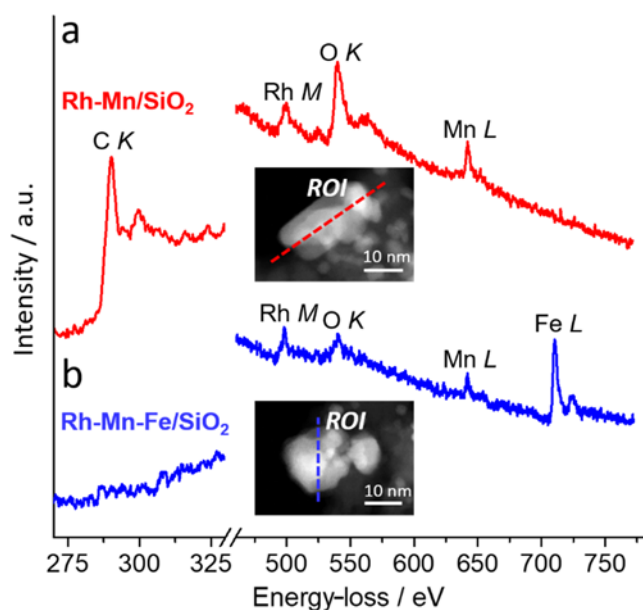


Figure 4. Comparison of STEM-EELS spectra recorded from sintered particles of postreaction (a) Rh-Mn@SiO₂ and (b) Rh-Mn-Fe@SiO₂ catalysts. O signal is from the SiO₂ support.

The strong Fe *L* edge (Figure 4b) shown in the spent Rh-Mn-Fe/SiO₂ catalyst again demonstrates the formation of a Rh-Fe alloy. The most notable difference of two spectra lies in the carbon *K* edge that is detected from the sintered particle of Mn promoted catalyst, while there is no carbon signal present on the Rh-Fe alloy particle of the bi-promoted catalyst. Further analysis reveals that the fine-structure of carbon *K* edge doesn't fit to either the finger-print of amorphous carbon or to the one of graphitic carbon.^[15] Instead, it is rather similar to that of carbides.^[16] EELS and EDX maps clearly reveal a similar distribution of C and Rh signals over the entire particle (Figure S16), unambiguously evidencing the formation of RhC_x. We have repeated this measurement on different sintered particles and they all show the same result: the formation of RhC_x exclusively occurs in the spent Rh-Mn/SiO₂ rather than in the spent Rh-Mn-Fe/SiO₂ catalysts (Figure S17). To the best of our knowledge, this is the first evidence of RhC_x formed in syngas upgrading. Thus, the Rh-Fe alloy shows higher resistance against the carbide formation, possibly due to the lower CO disassociation rate of this catalyst compared to the Rh-Mn/SiO₂ (Figure S1). The modified electronic properties of Rh in the Rh-Fe alloy may also lead to weakened absorption of carbonaceous species and an increased energy barrier for carbon diffusion,^[17] thus preventing the carbide formation.

Having identified Rh carbide in sintered particles in Rh-Mn/SiO₂ catalyst, we assessed if a similar phenomenon occurs on the smaller particles. However, the structural characterization of smaller particles by STEM provides no clear evidence for a RhC_x phase (Figure S6). On the other hand, it may be the case that some carbon atoms absorb in the sub-surfaces of the nanoparticles (Figure S6f) and owing to the low thickness of the sub-surfaces and low carbon content, the nanoparticles appear as a bulk metallic Rh. In order to examine whether the sub-surface RhC_x exists, we measured the carbon *K* edge of the small nanoparticles by EELS-line scan (Figure S18). The summarized

EELS spectra (Figure S18b,d) unambiguously reveal the presence of the carbon signal that could be ascribed to the carbidic structure (Figure S18e). The complementary study based on XPS reveals a slight change in the electronic structure of Rh in the spent Rh-Mn/SiO₂ catalyst (Figure S19), which could be related to the formation of RhC_x.

In conclusion, we have performed a detailed electron microscopy study of silica-supported Rh, Rh-Mn, and Rh-Mn-Fe catalysts of different states (calcined, reduced, spent), which provides not only the atomic-scale insight into the structural and chemical states of metal and promoters, but also insights about the metal-promoter interaction under reaction conditions. Our characterization reveals that in unpromoted calcined Rh catalyst, Rh exists as a crystalline oxide phase. Addition of promoters, either Mn alone or Mn and Fe together, leads to formation of complex oxides in which metal and promoters are in close proximity. In the best performing catalyst, *i.e.*, Rh-Mn-Fe/SiO₂, the metal and the promoters undergo a series of structural and chemical transformations. Due to the higher reducibility of Fe oxide compared to Mn oxide, the hydrogen spill-over from Rh only leads to a reduction of oxidic Fe to the metal state, followed by alloying with Rh. The alloying process is quite efficient, leading to incorporation of about 50% of Fe in Rh after reduction in hydrogen for 1 hour. After a long catalytic reaction (about 1 month), more than 70% of Fe is found in the bulk alloy form, instead of the surface alloy that was proposed in calculations.^[2, 5c, 5d] TEM characterization of the spent Rh-Mn catalyst also reveals the formation of Rh carbide in the catalytic CO hydrogenation process, which is however not detected in the Rh catalyst that contains both Mn and Fe. Hence, an additional role of Fe in preventing metal-catalyzed coking is uncovered in the process of syngas conversion over Rh-based catalysts.

Overall, analysis of Mn- and Mn-Fe-promoted, silica-supported Rh catalysts by TEM confirms the description of the active phase as a perforated core-shell structure on the support material, and reveals details of metal-promoter interaction at the atomic level. Our results provide a guideline for further development of DFT models of such catalysts for elucidation of the reaction mechanisms. Improved understanding of relations between catalyst structure and reaction induced modifications reported here provides a basis for a rational design of improved alcohol synthesis catalysts.

Acknowledgements

This work was conducted in the framework of the BasCat collaboration between BASF SE, Technical University Berlin, Fritz-Haber-Institut der Max-Planck-Gesellschaft, and the cluster of excellence "Unified Concepts in Catalysis" (UniCat www.unicat.tu-berlin.de).

Keywords: atomic-scale imaging • metal-promoter interaction • syngas-to-ethanol conversion • Rh-based catalysts • heterogeneous catalysis

- [1] a) J. J. Spivey, A. Egbeki, *Chem. Soc. Rev.* **2007**, 36, 1514-1528; b) Z. Fan, W. Chen, X. Pan, X. Bao, *Catal. Today* **2009**, 147, 86-93.

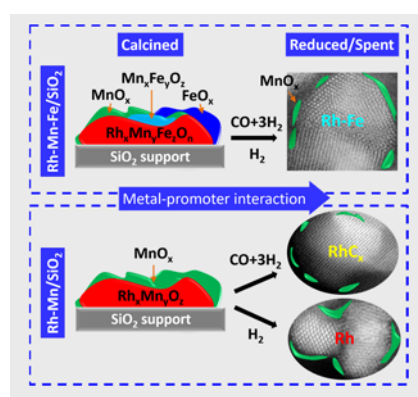
- [2] Y. Liu, F. Göeltl, I. Ro, M. R. Ball, C. Sener, I. B. Aragão, D. Zanchet, G. W. Huber, M. Mavrikakis, J. A. Dumesic, *ACS Catal.* **2017**, *7*, 4550-4563.
- [3] a) M. M. Bhasin, W. J. Bartley, P. C. Ellgen, T. P. Wilson, *J. Catal.* **1978**, *54*, 120-128; b) F. Li, W. Qian, *Appl. Petrochem. Res.* **2017**, *7*, 161-167.
- [4] a) M. Dimitrakopoulou, X. Huang, J. Krohnert, D. Teschner, S. Praetz, C. Schlesiger, W. Malzer, C. Janke, E. Schwab, F. Rosowski, H. Kaiser, S. A. Schunk, R. Schlögl, A. Trunschke, *Faraday Discuss.* **2018**, *208*, 207-225; b) W. Chen, Y. Ding, X. Song, T. Wang, H. Luo, *Appl. Catal., A* **2011**, *407*, 231-237; c) M. A. Haider, M. R. Gogate, R. J. Davis, *J. Catal.* **2009**, *261*, 9-16; d) F. G. A. van den Berg, J. H. E. Glezer, W. M. H. Sachtler, *J. Catal.* **1985**, *93*, 340-352; e) J. Liu, R. Tao, Z. Guo, J. R. Regalbuto, C. L. Marshall, R. F. Klie, J. T. Miller, R. J. Meyer, *ChemCatChem* **2013**, *5*, 3665-3672.
- [5] a) A. Medford, A. Lausche, F. Abild-Pedersen, B. Temel, N. Schjødt, J. Nørskov, F. Studt, *Top Catal* **2014**, *57*, 135-142; b) N. Yang, A. J. Medford, X. Liu, F. Studt, T. Bligaard, S. F. Bent, J. K. Nørskov, *J. Am. Chem. Soc.* **2016**, *138*, 3705-3714; c) Y. Choi, P. Liu, *J. Am. Chem. Soc.* **2009**, *131*, 13054-13061; d) I. A. W. Filot, F. Fariduddin, R. J. P. Broos, B. Zijlstra, E. J. M. Hensen, *Catal. Today* **2016**, *275*, 111-118.
- [6] a) N. Yang, J. S. Yoo, J. Schumann, P. Bothra, J. A. Singh, E. Valle, F. Abild-Pedersen, J. K. Nørskov, S. F. Bent, *ACS Catal.* **2017**, *7*, 5746-5757; b) M. Ojeda, M. L. Granados, S. Rojas, P. Terreros, F. J. García-García, J. L. G. Fierro, *Appl. Catal., A* **2004**, *261*, 47-55.
- [7] D. Mei, R. Rousseau, S. M. Kathmann, V.-A. Glezakou, M. H. Engelhard, W. Jiang, C. Wang, M. A. Gerber, J. F. White, D. J. Stevens, *J. Catal.* **2010**, *271*, 325-342.
- [8] a) D. S. Su, B. Zhang, R. Schlögl, *Chem. Rev.* **2015**, *115*, 2818-2882; b) D. Su, *Green Energy & Environ.* **2017**, *2*, 70-83; c) T. W. Hansen, J. B. Wagner, P. L. Hansen, S. Dahl, H. Topsøe, C. J. H. Jacobsen, *Science* **2001**, *294*, 1508-1510; d) M. D. Shannon, C. M. Lok, J. L. Casci, *J. Catal.* **2007**, *249*, 41-51.
- [9] R. Burch, M. I. Petch, *Appl. Catal., A* **1992**, *88*, 39-60.
- [10] J. Coey, *Acta Crystallogr., Sect. B* **1970**, *26*, 1876-1877.
- [11] C. C. Chao, P. Duwez, C. C. Tsuei, *J. Appl. Phys.* **1971**, *42*, 4282-4284.
- [12] R. M. Palomino, J. W. Magee, J. Llorca, S. D. Senanayake, M. G. White, *J. Catal.* **2015**, *329*, 87-94.
- [13] C. M. Wang, D. R. Baer, J. E. Amonette, M. H. Engelhard, J. Antony, Y. Qiang, *J. Am. Chem. Soc.* **2009**, *131*, 8824-8832.
- [14] M. C. Biesinger, B. P. Payne, A. P. Grosvenor, L. W. M. Lau, A. R. Gerson, R. S. C. Smart, *Appl. Surf. Sci.* **2011**, *257*, 2717-2730.
- [15] a) E. Willinger, A. Tarasov, R. Blume, A. Rinaldi, O. Timpe, C. Massué, M. Scherzer, J. Noack, R. Schlögl, M. G. Willinger, *ACS Catal.* **2017**, *7*, 4395-4407; b) H. Daniels, R. Brydson, B. Rand, A. Brown, *Philos. Mag.* **2007**, *87*, 4073-4092.
- [16] a) Y. Jin, H. Xu, A. K. Datye, *Microsc. Microanal.* **2006**, *12*, 124-134; b) L. P. Keller, *Meteoritics & Planetary Science* **1998**, *33*, 913-919.
- [17] J. Guo, C. Xie, K. Lee, N. Guo, J. T. Miller, M. J. Janik, C. Song, *ACS Catal.* **2011**, *1*, 574-582.

Entry for the Table of Contents (Please choose one layout)

Layout 1:

COMMUNICATION

Atomic insights about the metal-promoter interaction and the roles of promoters (Mn, Fe) in Rh-based catalysts for the syngas conversion to ethanol are provided based on a careful aberration-corrected high-resolution transmission electron microscopy study.



Xing Huang,* Detre Teschner, Maria Dimitrakopoulou, Alexey Fedorov, Benjamin Frank, Ralph Kraehnert, Frank Rosowski, Harry Kaiser, Stephan Schunk, Christiane Kuretschka, Robert Schlögl, Marc-Georg Willinger* and Annette Trunschke*

Page No. – Page No.

Atomic-Scale Observation of the Metal-Promoter Interaction in Rh-Based Syngas Upgrading Catalysts